Structural Optimization 8, 93–100 © Springer-Verlag 1994

Detecting delaminations in a composite beam using anti-optimization

J. Lee

Dept. of Engineering Science and Mechanics, Virginia Polytechnic Institute and State University, Blacksburg, VA 24061, USA

R.T. Haftka

Dept. of Aerospace and Ocean Engineering, Virginia Polytechnic Institute and State University, Blacksburg, VA 24061, USA

O.H. Griffin, Jr.

Dept. of Engineering Science and Mechanics, Virginia Polytechnic Institute and State University, Blacksburg, VA 24061, USA

L.T. Watson

Dept. of Computer Science and Mathematics, Virginia Polytechnic Institute and State University, Blacksburg, VA 24061, USA

M.D. Sensmeier

Dept. of Engineering Science and Mechanics, Virginia Polytechnic Institute and State University, Blacksburg, VA 24061, USA

Abstract The present study proposes a detection technique for delaminations in a laminated beam. The proposed technique optimizes the spatial distribution of harmonic excitation so as to magnify the difference in response between the delaminated and intact beam. The technique is evaluated by numerical simulation of two-layered aluminum beams. Effects of measurement and geometric noise are included in the analysis. A finite element model for a delaminated composite, based on a layer-wise laminated plate theory is used in conjunction with a step function to simulate delaminations

1 Introduction

Delamination is one of the most commonly observed damage modes in laminated composites and may develop as a result of manufacturing defects or in-service events such as low velocity impact. Delaminations are not readily identified by visual inspection since they are cracks in the interior of the laminate.

Delaminations are known to cause changes in vibration frequencies and mode shapes of laminated composites. The delaminated sublaminate generally exhibits new vibration modes and frequencies that depend on the size and location of the delamination. Thus, provided that the natural frequencies and mode shapes are known for a laminate containing delaminations, the presence of invisible delaminations can be detected, and their size and location can further be estimated.

Not much research has been done on detecting the existence and location of delaminations in laminated composites. Hanagud *et al.* (1992) proposed a method to detect a delamination in a laminated beam by comparing the vibration signature of a delaminated beam with an intact beam. They showed that it is difficult to assess the size and location of the delamination from the time response itself, and that care must be taken to calibrate the sensor response to detect the delaminations. Teboub and Hajela (1992) proposed a neural network based strategy for detecting delamination, fiber breakage, and matrix cracking in laminated composites. They computed the slopes of the strains at the measurement points by using piezoelectric sensors. Kim *et al.* (1993) used strain sensors on the surface and inside the material for detecting delaminations in laminated composites. Their results suggested that numerous sensors would be needed for large structures.

In the present paper, a finite element model based on a layer-wise laminated plate theory (Lee *et al.* 1992) is used to compute the steady state harmonic response of delaminated and intact beams. Then, an anti-optimization strategy is used in conjunction with system identification techniques for detecting a delamination. Anti-optimization is a method for maximizing differences between alternative models. Haftka and Kao (1990) maximized the ratio and difference between two laminated composite failure models by varying the loading, the geometry, and lamination angles. Gangadharan *et al.* (1991) sought the loads that maximize the difference in strain energies between two finite element models. They showed that the optimal discriminating loading was the solution to a generalized eigenvalue problem. Recently, Gangadharan *et al.* (1993) used an anti-optimization scheme for comparing alternative finite element models, and suggested that the method might be used to help damage detection.

In this paper, several measures of the difference between intact and delaminated beams are considered, including ratios of strain energies, external works, and surface strains. The ratios are maximized by solving eigenvalue problems. After obtaining the excitation that maximizes the response

ratio between delaminated and undelaminated beams, this excitation is used to detect the location of delamination as a force input in a residual force calculation.

2 Dynamic modelling of delamination

The notation here follows that of Lee *et al.* (1993). To model multiple delaminations, the layer-wise displacement field is supplemented with unit step functions which allow discontinuities in the displacement field (Fig. 1). The resulting displacements u_1 and u_3 at a generic point x, z in the laminate and time t are assumed to be of the form

$$u_1(x,z,t) = u(x,t) + \phi^j(z)u^j(x,t) + \delta^i(z)\overline{u}^i(x,t)\,,$$

$$u_3(x,z,t) = w(x,t) + \delta^i(z)\overline{w}^i(x,t)\,. \tag{1}$$

The superscripts i and j range from 1 to D and 1 to M, respectively, where D is the number of delaminations, and M is the number of layers of a composite. Repeated indices follow tensor notation for summation.

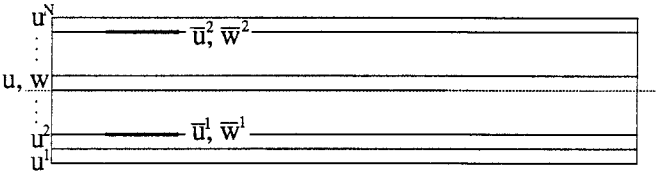

Fig. 1. Kinematics of layer-wise laminated composite plate theory

The terms u and w are the displacements of a point $(x,0,t)$ on the reference surface of the laminate, u^j are nodal values of the displacements in the x direction of each layer, $\overline{u}^i$ and $\overline{w}^i$ represent possible jumps in the slipping and opening displacements, respectively, at the $L(i)$-th delaminated interface, $L(i)$ denotes the location of the interface where the i-th delamination lies, and $\phi^j(z)$ and $\delta^i(z)$ denote a linear interpolation function through the thickness of the laminate and unit step function, respectively.

The Euler-Lagrange equations of motion of the layer-wise theory can be derived from Hamilton's principle

$$N_{x,x} = I^o\ddot{u} + I^j\ddot{u}^j + \overline{I}^i\ddot{\overline{u}}^i\,, \tag{2a}$$

$$Q_{xz,x} = I^o\ddot{w} + \overline{I}^i\ddot{\overline{w}}^i\,, \tag{2b}$$

$$N^j_{x,x} - Q^j_{xz} = I^j\ddot{u} + I^{jk}\ddot{u}^k + \tilde{I}^{ij}\ddot{\overline{u}}^i\,, \tag{2c}$$

$$\overline{N}^i_{x,x} = \overline{I}^i\ddot{u} + \tilde{I}^{ij}\ddot{u}^j + \overline{I}^{ir}\ddot{\overline{u}}^r\,, \tag{2d}$$

$$\overline{Q}^i_{xz,x} = \overline{I}^i\ddot{w} + \overline{I}^{ir}\ddot{\overline{w}}^r\,, \tag{2e}$$

where $i, r = 1, \ldots, D$ and $j, k = 1, \ldots, M$. The stress resultants are

$$[N_x, N^j_x, \overline{N}^i_x] = \int_{-h/2}^{h/2} \sigma_x[1, \phi^j, \delta^i]\,\mathrm{d}z\,,$$

$$[Q_{xz}, Q^j_{xz}, \overline{Q}^i_{xz}] = \int_{-h/2}^{h/2} \tau_{xz}[1, \phi^j_{,z}, \delta^i]\,\mathrm{d}z\,, \tag{3}$$

and the inertia coefficients are defined as

$$[I^o, I^j, \overline{I}^i] = \int_{-h/2}^{h/2} \rho[1, \phi^j, \delta^i]\,\mathrm{d}z\,,$$

$$[I^{jk}, \tilde{I}^{ij}, \overline{I}^{is}] = \int_{-h/2}^{h/2} \rho[\phi^j\phi^k, \delta^i\phi^j, \delta^i\delta^s]\,\mathrm{d}z\,, \tag{4}$$

where ρ is the material density. A more detailed mathematical formulation can be found in the paper by Lee *et al.* (1993).

To obtain finite element equations, the generalized displacements $(u, w, u^j, \overline{u}^i, \overline{w}^i)$ are expressed over each element as a linear combination of the one-dimensional interpolation functions ψ_ℓ and the nodal values:

$$(u, w, u^j, \overline{u}^i, \overline{w}^i) = \sum_{\ell=1}^{n} (u, w, u^j, \overline{u}^i, \overline{w}^i)_\ell \psi_\ell\,. \tag{5}$$

These expressions can then be used to develop the finite element model of a typical element. By assembling the element matrices, the global stiffness and mass matrices ($\mathbf{K}$ and $\mathbf{M}$) can be obtained.

3 Anti-optimization

The anti-optimization technique seeks conditions that maximize the difference between two models. Here we use anti-optimization to obtain the frequency and spatial distribution of excitations that maximize the difference between the delaminated and intact beams under harmonic excitation. First, consider the equations of motion of a delaminated beam under

$$\mathbf{M}\ddot{\mathbf{U}} + \mathbf{K}\mathbf{U} = \mathbf{H}\mathbf{f}e^{i\omega t}\,, \tag{6}$$

where ω denotes the excitation frequency, $\mathbf{M}$ and $\mathbf{K}$ are $n \times n$ mass and stiffness matrices, respectively, of a delaminated beam with n being the number of total degrees of freedom of the beam, $\mathbf{H}$ is a real matrix which indicates the locations of actuators, and $\mathbf{f}$ is an actuator input vector with dimension n.

Since the excitation is harmonic, so is the response

$$\mathbf{U} = \mathbf{u}e^{i\omega t}\,. \tag{7}$$

Thus, (6) becomes

$$(\mathbf{K} - \omega^2\mathbf{M})\mathbf{u} = \mathbf{H}\mathbf{f}\,. \tag{8}$$

To use anti-optimization, we need a measure of the difference in the response between the damaged and intact beams. In this work, we considered three possible measures as described below.

3.1 Strain energy measure

We started with the strain energy as a measure of the response. Therefore, we sought excitations that maximize the ratio E_1 of strain energies between delaminated and nominal structures

$$E_1 = \frac{\mathbf{u}^T\mathbf{K}\mathbf{u}}{\mathbf{u}_o^T\mathbf{K}_o\mathbf{u}_o}\,, \tag{9}$$

where $\mathbf{u}$ and $\mathbf{u}_o$ are the displacement vectors of delaminated and intact beams for a given excitation, respectively, and $\mathbf{K}_o$

is the stiffness matrix of an intact beam. We look for the excitation that maximizes E_1.

At the same time, the calculated displacement fields $\mathbf{u}$ should not be associated with very high natural frequencies, because such fields typically have small amplitudes and are difficult to measure. This imposes the constraint

$$E_2 = \frac{\mathbf{u}^T\mathbf{K}\mathbf{u}}{\mathbf{u}^T\mathbf{M}\mathbf{u}} < \omega_o^2 , \tag{10}$$

where ω_o is a limit frequency.

These two requirements can be combined by minimizing

$$\frac{1}{E_1} - \lambda\frac{1}{E_2} , \tag{11a}$$

or, alternatively, maximizing

$$E_3 = \frac{\mathbf{u}^T\mathbf{K}\mathbf{u}}{\mathbf{u}_o^T\mathbf{K}_o\mathbf{u}_o - \lambda\mathbf{u}^T\mathbf{M}\mathbf{u}} , \tag{11b}$$

where λ is a positive weighting factor. Since the frequency and spatial distribution of excitation is to be selected, (11b) is transformed in terms of excitation.

From (8), $\mathbf{u}$ can be obtained as

$$\mathbf{u} = (\mathbf{K} - \omega^2\mathbf{M})^{-1}\mathbf{H}\mathbf{f} . \tag{12}$$

Similarly for the undelaminated beam,

$$\mathbf{u}_o = (\mathbf{K}_o - \omega^2\mathbf{M}_o)^{-1}\mathbf{H}\mathbf{f} . \tag{13}$$

Now (11b) can be rewritten as

$$E_3 = \frac{\mathbf{f}^T\hat{\mathbf{K}}\mathbf{f}}{\mathbf{f}^T\hat{\mathbf{D}}\mathbf{f}} , \tag{14a}$$

where

$$\hat{\mathbf{K}} = \mathbf{H}^T(\mathbf{K} - \omega^2\mathbf{M})^{-1}\mathbf{K}(\mathbf{K} - \omega^2\mathbf{M})^{-1}\mathbf{H} ,$$

$$\hat{\mathbf{D}} = \hat{\mathbf{K}}_o - \lambda\hat{\mathbf{M}} ,$$

$$\hat{\mathbf{K}}_o = \mathbf{H}^T(\mathbf{K}_o - \omega^2\mathbf{M}_o)^{-1}\mathbf{K}_o(\mathbf{K}_o - \omega^2\mathbf{M}_o)^{-1}\mathbf{H} ,$$

$$\hat{\mathbf{M}} = \mathbf{H}^T(\mathbf{K} - \omega^2\mathbf{M})^{-1}\mathbf{M}(\mathbf{K} - \omega^2\mathbf{M})^{-1}\mathbf{H} , \tag{14b}$$

are generalized flexibility matrices associated with the two models. Equation (14a) indicates that E_3 is a Rayleigh quotient, so that its extreme values are the extreme eigenvalues of the generalized eigenvalue problem

$$(\hat{\mathbf{K}} - E_3\hat{\mathbf{D}})\mathbf{f} = 0 . \tag{15}$$

For a given set of actuator locations and excitation frequency, the actuator excitation amplitude vector that extremizes E_3 is the eigenvector of the eigenproblem of (15).

Stiffness and mass matrices of the delaminated beam ($\mathbf{K}$ and $\mathbf{M}$) are unknown in general, but $\hat{\mathbf{K}}$ and $\hat{\mathbf{M}}$ can be determined experimentally by measuring the displacements at the actuator locations as follows. The functional E_3 in (11b) can be rewritten using (8) as

$$E_3 = \frac{\mathbf{u}^T\mathbf{H}\mathbf{f} + \omega^2\mathbf{u}^T\mathbf{M}\mathbf{u}}{\mathbf{u}_o^T\mathbf{K}_o\mathbf{u}_o - \lambda\mathbf{u}^T\mathbf{M}\mathbf{u}} = \frac{\hat{\mathbf{u}}^T\mathbf{f} + \omega^2\mathbf{u}^T\mathbf{M}\mathbf{u}}{\mathbf{u}_o^T\mathbf{K}_o\mathbf{u}_o - \lambda\mathbf{u}^T\mathbf{M}\mathbf{u}} , \tag{16}$$

where $\hat{\mathbf{u}} = \mathbf{H}^T\mathbf{u}$ is a reduced displacement vector corresponding to the locations of actuators. Displacements at each actuator location of the beam need to be measured under the action of a unit load applied at each actuator, one at a time. The total displacement at each actuator location is then obtained as

$$\hat{u}_i = S_{ij}f_j , \tag{17}$$

where S_{ij} is the displacement generated at the i-th actuator location due to a unit load applied to the j-th actuator. The flexibility matrix $\mathbf{S}$ can be expressed with the aid of (12) as

$$\mathbf{S} = \mathbf{H}^T(\mathbf{K} - \omega^2\mathbf{M})^{-1}\mathbf{H} . \tag{18}$$

The quantity $\mathbf{u}^T\mathbf{M}\mathbf{u}$ can be determined from the derivative of $\mathbf{S}$ with respect to ω^2. That is,

$$\frac{\partial\mathbf{S}}{\partial(\omega^2)} = \mathbf{H}^T(\mathbf{K} - \omega^2\mathbf{M})^{-1}\mathbf{M}(\mathbf{K} - \omega^2\mathbf{M})^{-1}\mathbf{H} = \hat{\mathbf{M}} . \tag{19}$$

Therefore, we can write

$$\mathbf{u}^T\mathbf{M}\mathbf{u} = \mathbf{f}^T\frac{\partial\mathbf{S}}{\partial(\omega^2)}\mathbf{f} . \tag{20}$$

Note that the quantity $\partial\mathbf{S}/\partial\omega^2$ can be experimentally estimated by measuring $\mathbf{S}$ for several different frequencies ω. Finally, the functional $E_3 = \mathbf{f}^T\hat{\mathbf{K}}\mathbf{f}/\mathbf{f}^T\hat{\mathbf{D}}\mathbf{f}$ from (14a) is now expressed as

$$\hat{\mathbf{K}} = \mathbf{S} + \omega^2\frac{\partial\mathbf{S}}{\partial\omega^2} , \quad \hat{\mathbf{D}} = \hat{\mathbf{K}}_o - \lambda\frac{\partial\mathbf{S}}{\partial\omega^2} . \tag{21}$$

where $\mathbf{S}$ is measured for the damaged structure, and $\hat{\mathbf{K}}_o$ is calculated analytically from a model of the intact structure. If we do not have a good model of the intact structure, we can also measure $\hat{\mathbf{K}}_o$ as

$$\hat{\mathbf{K}}_o = \mathbf{S}_o + \omega^2\frac{\partial\mathbf{S}_o}{\partial\omega^2} , \tag{22}$$

where

$$\mathbf{S}_o = \mathbf{H}^T(\mathbf{K}_o - \omega^2\mathbf{M}_o)^{-1}\mathbf{H} . \tag{23}$$

3.2 External work measure

A second measure of the difference between two models is the ratio of work done by the external forces:

$$E_4 = \frac{\mathbf{u}^T\mathbf{H}\mathbf{f}}{\mathbf{u}_o^T\mathbf{H}\mathbf{f}} . \tag{24}$$

By using (12) and (13), E_4 can be written as

$$E_4 = \frac{\mathbf{f}^T\mathbf{S}\mathbf{f}}{\mathbf{f}^T\mathbf{S}_o\mathbf{f}} , \tag{25}$$

where

$$\mathbf{S}_o = \mathbf{H}^T(\mathbf{K}_o - \omega^2\mathbf{M}_o)^{-1}\mathbf{H} . \tag{26}$$

In the same manner as for the strain energy measure, maximizing E_4 can be written as an eigenvalue problem in which we seek the ratio of excitation corresponding to the largest eigenvalue E_4 of

$$(\mathbf{S} - E_4\mathbf{S}_o)\mathbf{f} = 0 . \tag{27}$$

3.3 Strain gauge measure

Because surface strains are easy to measure, we considered a third ratio involving only a vector $\boldsymbol{\epsilon}$ of surface strains. The anti-optimization approach is then used to maximize

$$E_5 = \frac{\|\boldsymbol{\epsilon}\|_2^2}{\|\boldsymbol{\epsilon}_o\|_2^2} , \tag{28}$$

where $\|\cdot\|_2$ denotes the Euclidean norm, and $\boldsymbol{\epsilon}$ and $\boldsymbol{\epsilon}_o$ are strain vectors of a delaminated and an undelaminated beam, respectively. Since the shear strain (γ_{xz}) vanishes at the top and bottom surfaces of the beam, $\boldsymbol{\epsilon}$ includes only normal strain (ϵ_x) components.

The measured strain at M locations of the delaminated beam is

$$\epsilon = \mathbf{GBu}, \tag{29}$$

where $\mathbf{G}$ contains sensor location information, and $\mathbf{B}$ is a differential operator which relates the strain vector to displacements. From (12) and (29) we obtain

$$\epsilon = \mathbf{Af}, \tag{30}$$

where

$$\mathbf{A} = \mathbf{GB}(\mathbf{K} - \omega^2\mathbf{M})^{-1}\mathbf{H} \tag{31}$$

is a matrix that relates the measured strains to the vector of external excitation for the delaminated beam. The matrix $\mathbf{A}$ can be determined experimentally by applying a unit load at each actuator, one at a time.

In the same manner, the strain vector of the intact beam is

$$\epsilon_o = \mathbf{A}_o\mathbf{f}, \tag{32}$$

where $\mathbf{A}_o$ is a matrix given by

$$\mathbf{A}_o = \mathbf{G}_o\mathbf{B}_o(\mathbf{K}_o - \omega^2\mathbf{M}_o)^{-1}\mathbf{H}. \tag{33}$$

Using (30) and (32), (28) can be finally written as

$$E_5 = \frac{\mathbf{f}^T\mathbf{Cf}}{\mathbf{f}^T\mathbf{C}_o\mathbf{f}}, \tag{34}$$

where

$$\mathbf{C} = \mathbf{A}^T\mathbf{A}, \quad \mathbf{C}_o = \mathbf{A}_o^T\mathbf{A}_o. \tag{35}$$

Maximization of (34) leads to the eigenvalue problem

$$(\mathbf{C} - E_5\mathbf{C}_o)\mathbf{f} = 0. \tag{36}$$

The generalized eigenvector $\mathbf{f}$, which corresponds to either the largest or smallest eigenvalue, is the excitation vector that maximizes the difference between delaminated and undelaminated beams as measured by the strain ratio E_5.

4 System identification

Once the excitation is found by anti-optimization, identifying the location of delamination in the structure is based on the differences in responses of delaminated and intact structures in conjunction with anti-optimization. Assume that the stiffness and mass matrices of a delaminated beam are written as

$$\mathbf{K} = \mathbf{K}_o + \eta_i\Delta\mathbf{K}_i, \quad \mathbf{M} = \mathbf{M}_o + \eta_i\Delta\mathbf{M}_i, \tag{37}$$

where η_i is an amplitude coefficient and $\Delta\mathbf{K}_i$ and $\Delta\mathbf{M}_i$ are differences in stiffness and mass matrices for the i-th delamination location, respectively. The subscript i indexes the simulated delaminations.

Using (37) and (13), we can define the residual force vector $\mathbf{R}$, which is similar to the one in the paper by Chen and Garba (1989), as

$$(\mathbf{K} - \omega^2\mathbf{M})\mathbf{u}_o - \mathbf{Hf} = \eta_i(\Delta\mathbf{K} - \omega^2\Delta\mathbf{M})_i\mathbf{u}_o \equiv \mathbf{R}. \tag{38}$$

The partial derivative of the residual force $\mathbf{R}$ with respect to the parameter η_i becomes

$$\frac{\partial\mathbf{R}}{\partial\eta_i} = (\Delta\mathbf{K} - \omega^2\Delta\mathbf{M})_i\mathbf{u}_o. \tag{39}$$

Observe that $(\Delta\mathbf{K} - \omega^2\Delta\mathbf{M})_i$ can be predetermined for all simulated delamination locations. The displacement vector of an intact structure $\mathbf{u}_o$ in (39) is calculated from (13) with an anti-optimization solution as a force vector $\mathbf{f}$. The partial derivatives of the residual force are calculated for all degrees of freedom of the beam, and later they are lumped into a parameter for each finite element node.

The delamination location is assumed to be the region where the derivative of residual force is high. When there is more than one peak in the residual force response, all the candidate locations are investigated further as follows: We find the maximum excitation ratio and corresponding eigenvector $\mathbf{f}^c$ for a given external frequency ω using the anti-optimization method described in the previous section for all candidates. Then the angles between the solution $\mathbf{f}$ of the original (measured) system with unknown delamination and the candidates $\mathbf{f}^c$ are calculated as

$$\theta = \arccos\left(\frac{|\mathbf{f}\cdot\mathbf{f}^c|}{\|\mathbf{f}\|\,\|\mathbf{f}^c\|}\right), \quad 0^\circ \le \theta \le 90^\circ. \tag{40}$$

The candidate whose eigenvector makes the smallest angle with the measured eigenvector is considered to be the actual location of delamination. After determining the delamination location, the delamination size can be estimated by comparing the eigenvalue of candidate size with the experimentally achieved eigenvalue.

5 Numerical example

A simply-supported aluminum beam of length $\ell = 3$ ft and thickness $h = 0.5$ in with a delamination at the midplane is considered for numerical investigation (Fig. 2); the material properties are

$$E = 10^7\text{psi}, \quad \nu = 0.3,$$

$$\rho = 0.1\frac{\text{lb m}}{\text{in}^3} = 0.259\times10^{-3}\frac{\text{lb}\cdot\text{s}^2}{\text{in}^4}. \tag{41}$$

A 7.2 in delamination (20% of the beam span) is assumed to be centered at the location $e/\ell = 0.3$. For criteria E_1 to E_4 we assume three pairs of force actuators and displacement sensors, spaced uniformly along the top surface of the beam. For criterion E_5 we assume that six sensors are attached on the bottom surface of the beam. Finite element analysis based on the theory described in the previous section is employed to solve the problem using 20 linear finite elements.

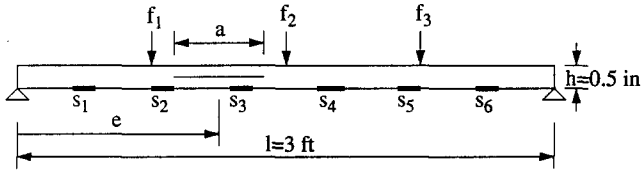

Fig. 2. Simply-supported beam with a delamination at midplane

5.1 *Natural frequencies*

The first ten natural frequencies of the beam are calculated and compared to those of its undelaminated counterpart in Table 1. There are no remarkable differences in frequencies between the two models for the first five modes. The 6th natural frequency of the delaminated beam (1140 Hz) is identified as the *delamination mode*, which is a nonclassical mode shape (Fig. 3). This special mode can lead to response differences from an undelaminated beam. However, as noted by Hanagud *et al.* (1992), it may be difficult to detect the size

and the location of the delamination from the time response data. Furthermore, it is not easy to assess the delamination by this high frequency excitation. Therefore, the actuator forces should be optimized such that the delaminated beam can be excited to maximize the response difference from the undelaminated beam even for low excitation frequencies.

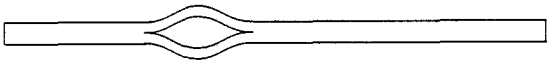

Fig. 3. Delamination mode at 1140.1 Hz

Table 1. Natural frequencies of delaminated and undelaminated beams

	Delaminated (Hz)	Undelaminated (Hz)
1	35.91	36.14
2	144.55	145.75
3	293.35	332.57
4	541.31	603.02
5	922.77	966.64
6	**1140.10**	1436.67
7	1207.85	2030.88
8	1751.60	2772.62
9	2390.73	2806.10
10	2800.28	3692.31

5.2 Weighting parameter

To show the effect of the weighting parameter λ, the response ratio E_3 was maximized for increasing values of λ by the eigenvalue problem (15). For each case, the corresponding values of E_1 and E_2 are given in Table 2. In this example, the excitation frequency (ω) was half of the first natural frequency of the undelaminated beam (ω_1).

For $\lambda = 0$ the value of E_2 falls between the square of the first (0.051×10^{-6}) and the second (0.825×10^{-6}) natural frequencies, which are not very high frequencies. Consequently, the displacement fields for $\lambda = 0$ are not associated with very high frequency vibration modes, and this λ value gives a reasonable approximation for strain energy anti-optimization. As λ increases, E_1 and E_2 approach 1 and the square of the first natural frequency, respectively. Substantial changes in E_1 and the eigenvector $\mathbf{f}$ do not occur until λ reaches 10^5. For all cases, the combined ratio E_3 was always found to be greater than 1.

Table 2. E_1 and E_2 ($\times10^6$) as functions of λ for excitation frequency equal to 0.5 ω_1

λ	E_1	E_2	f_1	f_2	f_3
0	1.364	0.653	-0.879	1	-0.481
10^3	1.364	0.589	-0.877	1	-0.478
10^4	1.300	0.144	-0.808	1	-0.418
10^5	1.023	0.051	-0.229	1	0.350

5.3 Comparison of response measures

Tables 3 (with $\lambda = 0$), 4 and 5 show the anti-optimization solutions of (15), (27), and (36), respectively, for various external frequencies. In these tables, both the maximum and minimum eigenvalues are calculated. Then, if the inverse ratio $1/E_i$ from the minimum eigenvalue is larger than E_i from the corresponding maximum eigenvalue, the entry is denoted by an asterisk (*) in the tables, and the eigenvector corresponding to the minimum eigenvalue is presented.

Table 3. Anti-optimization solution for excitation ratio using strain energy, eigenproblem (15) (with $\lambda = 0$). An asterisk denotes that the inverse of minimum eigenvalues is greater than maximum eigenvalues

ω/ω_1	max E_1	min E_1	Actuators f_1	f_2	f_3
0.5	1.364	0.999	-0.879	1	-0.481
0.95	2.410	0.726	-0.875	1	-0.513
0.99	74.56	0.132	-0.883	1	-0.529
1^{-a}	23.61	0.14×10^{-8}*	-0.890	1	-0.547
1.5	1.367	0.963	-0.871	1	-0.515
2	1.387	0.978	-0.919	1	-0.585
3	1.533	0.975	1	-0.640	0.780
5	2.055	0.887	1	0.617	0.937
10	3.457	0.122*	0.327	1	0.387

[a] 1^- indicates slightly smaller than one

For the strain energy ratio (Table 3), until the excitation frequency becomes very high ($\omega/\omega_1 = 10$), the maximum eigenvalue is greater than the inverse of the minimum eigenvalue except for frequencies very close to the resonant frequency. For $\omega/\omega_1 = 10$, the inverse of the minimum eigenvalue is greater than the maximum eigenvalue, and thus the eigenvector which corresponds to the minimum eigenvalue is considered in this case. For the external work ratio (Table 4), the minimum eigenvalue is always 1 for the frequencies lower than the first natural frequency ω_1. For $\omega > \omega_1$, the matrices $\mathbf{S}$ and $\mathbf{S}_o$ are not positive definite, and the minimum eigenvalue is less than 1. The inverse of the minimum eigenvalue becomes greater than the maximum eigenvalue for $\omega > \omega_1 = 10$ as for the strain energy case. In general, the eigenvalue seems less sensitive to the excitation frequency compared to the other approaches. The surface strain ratios show a different tendency, that is, even for low frequencies, the inverse of the minimum eigenvalue is greater than the maximum eigenvalue.

Table 4. Anti-optimization solution for excitation ratio using external work, eigenproblem (27). An asterisk denotes that the inverse of minimum eigenvalues is greater than maximum eigenvalues

ω/ω_1	max E_4	min E_4	Actuators f_1	f_2	f_3
0.5	1.363	1	-0.886	1	-0.478
0.95	1.498	1	-0.870	1	-0.481
0.99	3.511	1	-0.856	1	-0.487
1^-	1.067	-0.20×10^{-3}*	-0.845	1	-0.492
1.5	1.341	1	-0.858	1	-0.477
2	1.356	1	-0.832	1	-0.478
3	1.394	0.999	-0.764	1	-0.478
5	1.404	0.984	-0.562	1	-0.479
10	1	0.389*	0.028	1	-0.492

For all methods, when the excitation frequency approaches the first resonant frequency from below, the max-

imum eigenvalue increases by an order of magnitude and the minimum eigenvalue decreases, while the corresponding eigenvectors do not change much. When the external frequency is very close to the first natural frequency from below, the maximum eigenvalue decreases rather sharply and the minimum eigenvalue decreases drastically to almost zero. The eigenvector in this case is presented for the minimum eigenvalue, but it appears that the eigenvalue for this case is almost same as the one for $\omega/\omega_1 = 0.99$, which corresponds to the maximum eigenvalue. This shows that as the resonant frequency is approached, the eigenvector for the two extreme eigenvalues converge [observe that at the resonant frequency ($\omega = \omega_1$), the matrix $\mathbf{C}_o = \mathbf{A}_o^T \mathbf{A}_o$ is not defined since the matrix $\mathbf{K}_o - \omega^2 \mathbf{M}_o$ in $\mathbf{A}_o$ is singular, see (33)].

For higher excitation frequencies, high ratios are obtained for all approaches. This suggests that the higher the frequency, the higher the ratio if the excitation frequency is not close to the resonant frequencies. However, for measurement purposes, very high frequencies are not recommended.

The results from the strain energy are, in general, more reliable than those from strain sensors, because strain energy is calculated at every degree of freedom of the finite element mesh of the beam, while strains are measured at several points on the surface of the beam. For example, at $\omega/\omega_1 = 5$, the difference in ratio between two approaches is about 30%. The strain energy results are also more efficient (larger values of ratios) than those from external work for all the excitation frequencies.

Table 5. Anti-optimization solution for excitation ratio using strain sensor, eigenproblem (36). An asterisk denotes that the inverse of minimum eigenvalues is greater than maximum eigenvalues

ω/ω_1	max	min	Actuators		
	E_5	E_5	f_1	f_2	f_3
0.5	1.020	0.913*	1	-0.688	0.173
0.95	2.107	0.579	-0.851	1	-0.531
0.99	77.120	0.089	-0.862	1	-0.550
1^-	25.021	0.93×10^{-9}*	-0.860	1	-0.554
1.5	1.081	0.866*	1	-0.811	0.746
2	1.094	0.900*	1	-0.430	-0.853
3	1.243	0.917	-0.299	1	-0.070
5	1.549	0.701	0.752	1	0.593
10	5.811	0.029*	0.449	1	0.498

The effect of the number of strain sensors on the optimum solution is investigated for $\omega/\omega_1 = 5$ in Table 6. Strain sensors are assumed to be uniformly spaced. As expected, the results approach the strain energy results with an increasing number of sensor results. As a result, strain energy measure is found to be the most efficient and accurate. For this reason, in the following the strain energy is used as the response measure for anti-optimization.

5.4 Effects of errors

In many practical situations, measurement noise and modelling errors may be significant. To simulate such noise and errors, the actuator amplitude vector ($\mathbf{f}$) and matrix $\hat{\mathbf{K}}$ in (21) calculated from the strain energy anti-optimization are perturbed as follows:

Table 6. Effect of the number of strain sensors for $\omega/\omega_1 = 5$

Number of strain sensors		Actuators		
	E_5	f_1	f_2	f_3
3	3.816	0.710	1	0.689
4	2.738	1	-0.207	0.899
6	1.549	0.752	1	0.593
10	1.870	1	0.512	0.908
20	1.982	1	0.616	0.931
Strain energy solution	$E_1 = 2.055$	1	0.617	0.937

$$\mathbf{f}_i = [1 + N(2R-1)]\mathbf{f}_i, \quad \hat{K}_{ij} = [1 + N(2R-1)]\hat{\mathbf{K}}_{ij}, \tag{42}$$

where N is a noise amplitude and R is a random number uniformly distributed between zero and one. First, actuator amplitude vectors are perturbed, and the mean values of relative errors of two extreme eigenvalues are presented in Table 7 for four different excitation frequencies. The relative errors in Table 7 are defined as

$$\Delta E = \frac{|E_{\text{perturbed}} - E_{\text{exact}}|}{E_{\text{exact}}}. \tag{43}$$

It is seen that both maximum and minimum eigenvalues are not sensitive to measurement noise except very close to a resonant frequency. This is because in this case, the eigenvector of the minimum eigenvalue [$\mathbf{f}$ = (-0.889, 1, -0.547)] is very close to that of the maximum eigenvalue [$\mathbf{f}$ = (-0.883, 1, -0.529)]. Thus, even small perturbation in eigenvectors can cause a very large deviation in eigenvalues.

Table 7. Effects of perturbed eigenvector on relative errors in strain energy ratio E_1

ω/ω_1	1% Noise		5% Noise	
	$\Delta E_{\min}$	$\Delta E_{\max}$	$\Delta E_{\min}$	$\Delta E_{\max}$
0.5	0.46×10^{-5}	0.13×10^{-3}	0.12×10^{-3}	0.32×10^{-2}
0.99	5.98	0.29	122.42	0.73
2	0.58×10^{-6}	0.20×10^{-4}	0.14×10^{-4}	0.50×10^{-3}
5	0.12×10^{-4}	0.17×10^{-3}	0.32×10^{-3}	0.41×10^{-2}

In general, beams are not perfect and have variations in material properties and geometry. We simulate such imperfections through random thickness variation along the beam length. The thickness of each finite element is allowed to vary within 5% combined with the variation of matrix $\hat{\mathbf{K}}$. The relative errors of two extreme eigenvalues and the angles between exact and perturbed eigenvectors are presented in Table 8. For $\omega/\omega_1 = 0.5$, the results are shown to be sensitive to the variation of $\hat{\mathbf{K}}$ with more than 1% noise of measurement error producing unacceptable errors. At excitation frequencies close to resonance, the results are too sensitive to be meaningful. This is because of the unstable nature of the $\hat{\mathbf{K}}$ matrix near resonance. Thus, this excitation frequency is not appropriate for identification. For higher excitation frequencies, the results are much less sensitive to the measurement noise. For $\omega/\omega_1 = 2$, the angle between exact and perturbed eigenvectors is only 3° even for 5% measurement noise. This excitation frequency is found to be the best among the frequencies considered. For all cases, the effect of thickness variation seems to be negligible compared to the measurement noise.

Table 8. Effects of geometric and measurement noise on relative errors in strain energy ratio E_1 and change θ (in degrees) in angle of anti-optimized force vector

ω/ω_1	Noise in $\hat{\mathbf{K}}$	No thickness variation			5% thickness variation		
		$\Delta E_{\min}$	$\Delta E_{\max}$	θ	$\Delta E_{\min}$	$\Delta E_{\max}$	θ
0.5	0%	0	0	0	0.015	0.001	0.325
	1%	0.199	0.063	12.53	0.207	0.067	13.05
	3%	0.501	0.291	26.30	0.528	0.306	26.85
	5%	0.850	0.544	29.47	0.857	0.546	29.50
0.99	0%	0	0	0	31.87	0.001	0.343
	1%	9590	23.01	34.08	12840	22.83	31.66
2	0%	0	0	0	0.014	0.001	0.364
	1%	0.015	0.002	0.576	0.019	0.002	0.675
	3%	0.047	0.008	1.780	0.049	0.008	1.814
	5%	0.078	0.016	2.988	0.079	0.017	3.043
5	0%	0	0	0	0.055	0.018	0.975
	1%	0.108	0.025	2.560	0.109	0.028	2.625
	3%	0.297	0.061	7.958	0.300	0.062	8.310
	5%	0.479	0.116	14.29	0.486	0.117	14.35

5.5 Delamination detection

The actuator magnitude ratios that maximize the strain energy ratio are obtained for three different excitation frequencies. The derivative of the residual force is calculated for every possible simulated delamination with a size of 10% of the beam length from node 1 to node 21, and is plotted through the axial location of the beam in Fig. 4 both with and without measurement noise in $\hat{\mathbf{K}}$. For each finite element node, these three values are multiplied to help find peaks. Results are presented in Fig. 5. There are two peaks in Fig. 5, and the delaminated region is indicated to be either of these two locations of the beam. The effect of noise is negligible as can be seen from Figs. 4 and 5.

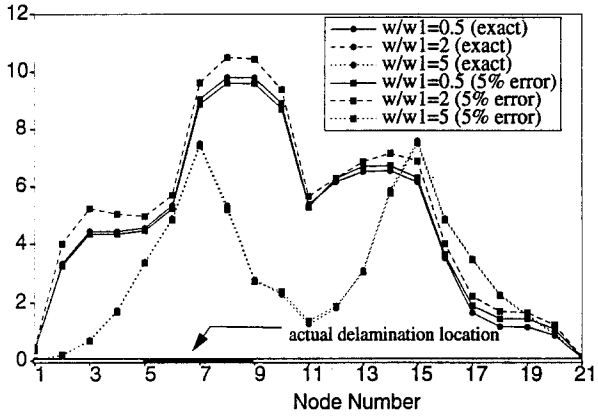

Fig. 4. The derivative of residual force for a delamination at e/ℓ = 0.3

It should be noted that the location corresponding to the higher peak is not necessarily the location of delamination. Thus, both candidate locations of delamination are further investigated by using the method described in Section 4. The location of C_1 and C_2 can be estimated based on Fig. 5 as

C_1 : delaminated at node 7 ,

C_2 : delaminated at node 15 . (44)

The eigenvectors for the two candidates are calculated by using anti-optimization, and the angles for both candidates are presented in Table 9 for the three different excitation

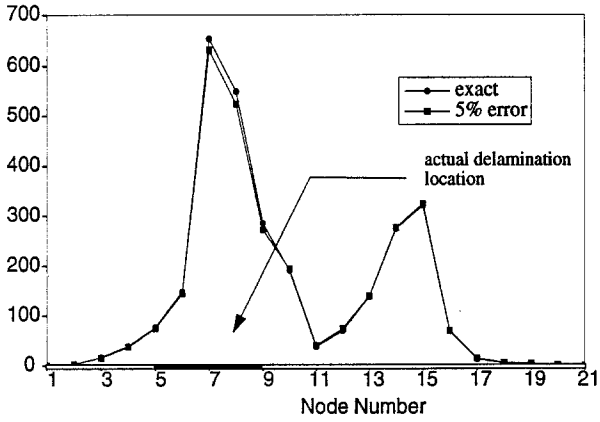

Fig. 5. The derivative of residual force for a delamination at e/ℓ = 0.3 (multiplied)

frequencies. The angles associated with C_1 are smaller for three frequencies.

Table 9. Estimation of the location of a delamination

Candidate	ω/ω_1	E_3	Actuators			θ
			f_1	f_2	f_3	
C_1 (node 7)	0.5	1.051	-0.894	1	-0.474	0.605
	2	1.053	-0.948	1	-0.605	0.908
	5	1.146	1	0.736	0.927	4.128
C_2 (node 7)	0.5	1.051	-0.474	1	-0.894	23.517
	2	1.053	-0.605	1	-0.948	18.487
	5	1.146	0.927	0.736	1	5.480

In fact, neither C_1 nor C_2 corresponds exactly to the actual location and size of delamination. For low excitation frequencies, the error angle θ between the actual location and the C_1 is small. As the frequency increases, the angle becomes larger for C_1, but the error angle for C_2 decreases. This is because C_2 has a mirror image to the actual delamination location and becomes indistinguishable for larger wave numbers. That is, for more accurate estimation of delamination location, higher frequencies may be necessary, whereas low frequencies are preferable for selecting a candidate that is closer to actual delamination location. Consequently, C_1 is the estimated location of delamination.

Once the location of a delamination is estimated, the next step is to determine the size of the delamination. The delamination size can be estimated by comparing the measured eigenvalues with eigenvalues of candidate delaminations. These candidates are produced by increasing the size of the delamination by releasing neighbouring nodes of C_1. As shown in Table 10, it can be concluded that any of the entries except the one with only node 7 delaminated can be a solution (observe ΔE).

6 Concluding remarks

In this paper, a technique that can detect a delamination in laminated beams was presented. Using anti-optimization, an optimal excitation load distribution, which extremizes the difference between harmonic response of a nominal and delaminated beams, was obtained. Then, the location and the size of a delamination is then estimated by using the excitation obtained from anti-optimization in conjuction with

Table 10. Estimation of the size of a delamination

Delaminated nodes	E_3	Actuators			ΔE_3
		f_1	f_2	f_3	
7	1.051	-0.894	1	-0.474	0.235
6,7	1.112	-0.867	1	-0.485	0.185
7,8	1.208	-0.897	1	-0.473	0.114
5,6,7	1.179	-0.920	1	-0.461	0.136
6,7,8	1.364	-0.879	1	-0.481	0
7,8,9	1.524	-0.9	1	-0.474	0.117

system identification. In order to validate the reliability of the approach, geometric and measurement noise effects were numerically simulated. It was found that the present anti-optimization based system identification technique is capable of detecting the size and the location of delamination successfully. Experimental work to verify this capability is currently underway and will be reported in another publication.

The significance of the anti-optimization procedure detailed in this paper lies in its ability to augment the system identification process. Most system identification approaches require large amounts of data to detect damage. By accentuating the difference between the response of nominal and delaminated beams, anti-optimization reduces the amount of data required to detect the damage.

Acknowledgement

The authors gratefully acknowledge the support of the Army Research Office University Research Initiative Center Program, Grant No. DAAL 03-92-G-0180; Dr. Gary Anderson, Program Manager.

References

Chen, J.C.; Garba, J.A. 1989: On-orbit damage assessment for large space structures. *AIAA J.* **26**, 1119-1126

Gangadharan, S.N.; Nikolaidis, E.; Haftka, R.T. 1991: Probabilistic system identification of two flexible joint models. *AIAA J.* **29**, 1319-1326

Gangadharan, S.N.; Nikolaidis, E.; Lee, K.; Haftka, R.T. 1993: The use of anti-optmization to compare alternative structural models. Presented at the 34th AIAA/ASME/ASCE/AHS/ASC SDM Conf. (held in La Jolla, CA)

Haftka, R.T.; Kao, P.J. 1990: The use of optimization for sharpening differences between models. Paper presented at the ASME Winter Annual Meeting (held in Dallas, TX)

Hanagud, S.; Babu, G.L.N.; Roglin, R.L.; Savanur, S.G. 1992: Active control of delaminations in composite structures. Presented at the 33th AIAA/ASME/ASCE/AHS/ASC SDM Conf. (held in Dallas, TX)

Kim, K.; Segall, A.; Springer, G. 1993: The use of strain measurements for detecting delaminations in composite laminates. *Comp. & Struct.* **23**, 75-84

Lee, J.; Gürdal, Z.; Griffin, O.H. 1993: Composites with delaminations. *AIAA J.* **31**, 331-338

Teboub, Y.; Hajela, P. 1992: A neural network based damage analysis of smart composite beams. Presented at the 4th AIAA/USAF/NASA/OAI Symp. Multidisplinary Analysis and Optimization (held in Cleveland, OH)

Received April 28, 1994
Communicated by J. Sobieski